eprints@whiterose.ac.uk
https://eprints.whiterose.ac.uk/

Optimum Lateral Load Distribution for Seismic Design of Nonlinear Shear-Buildings Considering Soil-Structure Interaction

Behnoud Ganjavi[1*], Iman Hajirasouliha[2], Ali Bolourchi[3]

[1] *Department of Civil Engineering, University of Mazandaran, Babolsar, Iran*

[2] *Department of Civil and Structural Engineering, University of Sheffield, Sheffield, UK*

[3] *Department of Civil and Environmental Engineering, University of Southern California, California, USA*

* *Corresponding author: b.ganjavi@umz.ac.ir*

Abstract

The lateral load distributions specified by seismic design provisions are primarily based on elastic behaviour of fixed-base structures without considering the effects of soil-structure-interaction (SSI). Consequently, such load patterns may not be suitable for seismic design of non-linear flexible-base structures. In this paper, a practical optimization technique is introduced to obtain optimum seismic design loads for non-linear shear-buildings on soft soils based on the concept of uniform damage distribution. SSI effects are taken into account by using the cone model. Over 30,000 optimum load patterns are obtained for 21 earthquake excitations recorded on soft soils to investigate the effects of fundamental period of the structure, number of stories, ductility demand, earthquake excitation, damping ratio, damping model, structural post yield behaviour, soil flexibility and structural aspect ratio on the optimum load patterns. The results indicate that the proposed optimum load patterns can significantly improve the seismic performance of flexible-base buildings on soft soils.

Keywords: Soil-Structure Interaction; Optimum strength distribution; Uniform damage distribution; Inelastic behaviour; Seismic code; Soft soil

1. INTRODUCTION

The preliminary design of regular building structures in current seismic design codes is commonly based on the equivalent static force approach, in which the dynamic inertial forces due to seismic vibrations are represented by equivalent static forces (force-based design procedure). The height-wise

distribution of the seismic design static forces in different standards is usually only a function of fundamental period of the structure and the height-wise distribution of structural mass (e.g. EuroCode 8 [1], International Building Code 2012 [2], ASCE/SEI 7-10 [3], NEHRP 2003 [4], Uniform Building Code [5]). This implies that the equivalent static forces are derived primarily based on the elastic dynamic response of fixed-base structures without considering soil-structure interaction (SSI) effects. The efficiency of using the code-specified lateral load patterns for fixed-base building structures has been extensively investigated [6-15]. The results of these studies indicated that the current design approach, in general, does not lead to a uniform distribution of deformation demands in multi-story structures.

Leelataviwat et al. [9] evaluated the seismic demands of mid-rise moment-resisting frames designed in accordance with Uniform Building Code [5]. They proposed improved load patterns using the concept of energy balance applied to moment-resisting frames with a pre-selected yield mechanism. Using the same concept, Lee and Goel [16] proposed new seismic lateral load patterns for high-rise moment-resisting frames (up to 20 stories). However, they dealt with a limited number of ground motions. Their proposed load pattern fundamentally follows the shape of the lateral load pattern in the Uniform Building Code [5] and is a function of the mass and the fundamental period of the structure. In a more comprehensive research, Mohammadi et al. [10] investigated the effect of design lateral load patterns on drift and ductility demands of fixed-base shear building structures under 21 earthquake ground motions. Their results indicate that using the code-specified design load patterns do not generally lead to a uniform distribution of story ductility demands. Ganjavi et al. [16] investigated the effect of using equivalent static and spectral dynamic lateral load patterns specified by the conventional seismic codes on height-wise distribution of drift, hysteretic energy and damage index of fixed-base reinforced concrete buildings subjected to severe earthquakes. They concluded that none of the code-based design load patterns leads to a uniform distribution of drift, hysteretic energy and structural damage under strong earthquakes. It was also observed that in the structures designed using the equivalent static method these performance parameters can be much higher in one or two stories (i.e. soft story phenomenon). More recently, several studies have been conducted to evaluate and improve the code-specified design lateral load patterns based on the inelastic behaviour of the structures [e.g. 11, 15, 17, 18]. However, none of the above studies considered the effects of SSI.

Several studies investigated the effects of SSI on elastic and inelastic response of buildings [19-27]. In general, the results of these studies demonstrated that SSI can significantly affect the seismic response of structures located on soft soils by altering the overall stiffness and energy dissipation mechanism of the systems. Compared to fixed-base systems, soil-structure systems possess longer periods and generally higher damping ratios due to the energy dissipation provided by hysteretic behaviour and wave radiation in the soil medium. Ganjavi and Hao [28] investigated the adequacy of IBC-2009 lateral loading patterns

for seismic design of elastic and inelastic soil-structure systems through analyses of 7200 shear-buildings with SSI effects subjected to a group of 30 earthquakes recorded on alluvium and soft soils. They concluded that using the code-specified design load patterns leads to nearly uniform ductility demand distributions for structures having short periods and within the elastic range of response. For structures with longer periods, however, the efficiency of the IBC design load pattern was considerably reduced, which was more evident by increasing the soil flexibility and the story ductility demands. In another study, Ganjavi and Hao [29] developed a new optimization algorithm for optimum seismic design of elastic shear-building structures with SSI effects. Their adopted optimization method was based on the concept of uniform damage distribution proposed by Moahammadi et al. [10] and Moghadam and Hajirasouliha [11, 12] for fixed-base shear building structures. Based on the results of their study, Ganjavi and Hao [29] proposed a new design lateral load pattern for seismic design of elastic soil-structure systems, which can lead to a more uniform distribution of deformations and up to 40% less structural weight as compared with code-compliant structures. However, their proposed load pattern was developed only for elastic SSI systems and, therefore, may not be applicable for non-linear structures on soft soils. Through performing a parametric study on nonlinear shear-buildings with SSI effects, Bolourchi [30] showed that SSI can significantly affect optimum lateral load patterns when compared to the corresponding fixed-base systems. However, the results of that study were based on very limited fixed-base fundamental periods and earthquake ground motions, and also the soil-structure systems were modelled using cone model with frequency independent impedances in which no material damping was considered.

This study aims to provide a fundamental step towards the development of a more rational seismic design methodology that explicitly accounts for the complex phenomenon of soil-structure interaction and inelastic behaviour of structures. The optimization algorithm adopted by Ganjavi and Hao [29] to obtain optimum design load patterns for elastic soil-structure systems is further developed to incorporate the inelastic behaviour of structures. By performing extensive numerical simulations on a wide range of inelastic soil-structure systems, the effects of fundamental period of the structure, number of stories, slenderness ratio, maximum ductility demand, earthquake excitation, damping ratio, damping model, structural post yield behaviour and soil flexibility on optimum design load patterns are investigated. The efficiency of the proposed optimum load patterns is demonstrated through several design examples.

2. MODELLING OF SUPERSTRUCTURES AND SELECTED GROUND MOTIONS

In this study, superstructures are modelled based on the procedure proposed by FEMA 440 [31], which allows engineers model certain complex structures as MDOF shear buildings. Shear building models can

3

represent multi-story structures with shear beams or those with relatively stiff diaphragms with respect to columns. In spite of some drawbacks, these models have been widely used to study the seismic response of multi-story buildings because of simplicity and low computational effort that enables a wide range of parametric studies [e.g. 14, 25, 27, 29, 30]. In MDOF shear-buildings, floors are modelled as lumped masses which are connected by elasto-plastic springs. As shown in Figure 1 (a), in this study a bilinear elasto-plastic model with 2% post-yield strain hardening is used to represent the story lateral stiffness of each floor. The effect of using different strain hardening ratios is also investigated in this study. This model is selected to represent the behaviour of non-deteriorating steel-framed structures with high beam-to-column stiffness ratio. However, moment resisting frames with high beam-to-column stiffness ratio may not comply with current seismic design provisions to enforce the formation of plastic hinges in the beams. It should be noted if member joints and connections are not well detailed, steel-framed structures may exhibit some cyclic strength and stiffness degradation that can influence their seismic performance under strong earthquakes. In the present study, there effects are not taken into account.

Story heights are considered to be 3 meters and the mass of the structure is uniformly distributed over the height (i.e. all stories have the same lumped mass). In all MDOF models, lateral story stiffness is assumed to be proportional to the story shear strength distributed over the height of the structure [14, 15]. The height-wise strength distribution is obtained in accordance with the selected lateral design load pattern. Five percent Rayleigh damping is assigned to the first mode and the mode in which the cumulative mass participation is at least 95%. In this study, the effect of different structural damping ratios and damping models on the optimum lateral load patterns are also studied.

In this investigation, an ensemble of 21 earthquake ground motions recorded on alluvium and soft soil deposits (shear wave velocity ranging from 100 to 350 m/s) is employed as listed in Table 1. The selected ground motions are components of six strong earthquakes with magnitude greater than 6 including Imperial Valley 1979, Morgan Hill 1984, Superstition Hills 1987, Loma Prieta 1989, Northridge 1994 and Kobe 1995. The selected records do not show pulse type behaviour and are obtained from earthquakes having the closest distance to fault rupture more than 15 km. To provide reliable results for design purposes, SeismoMatch software [32] was used to adjust the selected seismic ground motion records to the elastic design response spectrum of IBC-2012 with soil type *E*. The spectrum compatible earthquakes can represent the design response spectrum and therefore are suitable for general design purposes [15]. SeismoMatch is capable of adjusting earthquake accelerograms to match a specific target response spectrum using wavelets algorithm, which preserves the high-frequency characteristics of the input ground motion that are important for engineering projects [33]. Figure 1 (b) shows the good agreement between the response spectra of the 21 adjusted ground motions with the target elastic design response spectrum of IBC-2012.

3. SOIL MODEL

In this study, the cone model is adopted to simulate the dynamic behaviour of an elastic homogeneous soil half-space [34]. The model is based on one-dimensional wave propagation theory and can represent a circular rigid foundation with mass m_f and mass moment of inertia I_f resting on a homogeneous half-space soil. The cone model has been widely used for modelling both surface and embedded foundations and, in lieu of the rigorous elasto-dynamical approach, can provide sufficient accuracy for engineering design purposes [35]. A general substructure method is used to model the soil-structure systems in this study. In this approach, soil is modelled separately and then it is combined with the structure model to establish the full soil-structure system. The soil-foundation system is modelled by an equivalent linear discrete model based on the cone model approach with frequency-dependent coefficients [34]. The foundation is considered as a circular rigid disk (the flexibility of the foundation is not taken into account). The foundation mass, m_f, is assumed such that the foundation uplift does not occur under the design earthquake loads according to ASCE 7-10 [3]. The kinematic interaction effect is not included assuming that the rigid foundation lies on the surface of the soil with no embedment.

Figure 2 shows a typical 4-story shear-building model of fixed-base and flexible-base systems used in this study. The sway (h) and rocking (φ) degrees of freedom are defined as representatives of translational and rocking motions of the shallow foundation, respectively, disregarding the slight effect of vertical and torsional motion. The stiffness and energy dissipation characteristics of the supporting soil are represented by springs and dashpot, respectively. In addition, while being hysteretic inherently, soil material damping is assumed as commonly used viscous damping to avoid complexity in time-domain analysis. In SSI models, u_h and φH_n indicate the horizontal displacement components caused by the sway and the rocking motions at the roof story, respectively, and u_r is associated with the shear deformation of the superstructure. To model the frequency-dependent rotational spring and dashpot coefficients, an additional internal rotational degree of freedom, θ, is assigned to a polar mass moment of inertia, m_θ, and connected to the foundation mass with a zero-length element using a rotational dashpot [27-29]. Moreover, to modify the effect of soil incompressibility, an additional mass moment of inertia ΔM_φ is added to the foundation when υ is greater than 1/3 [34]. In this case, the dilatational shear wave velocity, V_p, is limited to $2V_s$ [35]. The coefficients of the sway and rocking springs and dashpots used to define soil-shallow foundation models in Figure 2 (b) are summarized as follows:

$$k_h = \frac{8\rho V_s^2 r}{2-\upsilon}, \qquad c_h = \rho V_s A_0 \tag{1}$$

$$k_\varphi = \frac{8\rho V_s^2 r^3}{3(1-\upsilon)}, \qquad c_\varphi = \rho V_p I_0 \tag{2}$$

$$m_\theta = \frac{9\pi\rho r^5}{128}(1-\upsilon)\left(\frac{V_p}{V_s}\right)^2 \tag{3}$$

$$\Delta M_\varphi = 0.3\pi(\upsilon - 1/3)\rho r^5 \tag{4}$$

where k_h, c_h, k_φ and c_φ are sway stiffness, sway viscous damping, rocking stiffness, and rocking viscous damping, respectively. Equivalent radius and area of cylindrical foundation are denoted by r and A_0. Besides, ρ, υ, V_p and V_s are, respectively, the specific mass density, Poisson's ratio, dilatational and shear wave velocity of soil. To consider the soil material damping, ζ_0, each spring and dashpot of the soil-foundation model is, respectively, augmented with an additional parallel connected dashpot and mass. It is known that the shear modulus of the soil decreases as soil strain increases. In this study, the effect of soil nonlinearity on the soil-foundation element is approximated through utilising a degraded shear wave velocity, compatible with the estimated strain level in the soil medium [36]. This approach is currently used in the modern seismic provisions such as NEHRP 2003 [4] and FEMA 440 [31], where the strain level in the soil medium is implicitly related to the peak ground acceleration (PGA).

4. GOVERNING INTERACTING PARAMETERS

The seismic response of a soil-structure system essentially depends on the size of the structure, dynamic characteristics of the soil and structure, soil profile as well as the applied excitation. For a specific earthquake ground motion, the dynamic response of the structure can be interpreted based on the properties of the superstructure relative to the soil beneath it. It has been shown that the effect of these factors can be best described by two parameters: non-dimensional frequency and aspect ratio [37]. To consider soil flexibility in a given system, non-dimensional frequency a_0 is defined as an index for the structure-to-soil stiffness ratio $a_0 = (\omega_{fix}\bar{H})/V_s$, where ω_{fix} and $\bar{H}$ denote the circular frequency of the fixed-base structure and the effective height of the superstructure, respectively. The results of Stewart et al. [38] study imply that by increasing a_0, the effects of SSI would be generally more significant. It can be shown that the practical range of a_0 for conventional building structures is from zero for fixed-base structures to about 3 for the structures with severe SSI effects [19].

The effective height of a MDOF structure $\bar{H}$ is defined as the height to the centre of the lateral seismic forces such that the overturning moment in the equivalent SDOF system is the same as the original

structure. The effective height $\bar{H}$ corresponding to the fundamental mode properties of a MDOF building can be obtained from the deflected shape and mass distribution using the following equation [8]:

$$\bar{H} = \frac{\sum_{j=1}^{n}\left[m_j \varphi_{j1}\left(\sum_{i=1}^{j} h_i\right)\right]}{\sum_{j=1}^{n} m_j \varphi_{j1}} \tag{5}$$

where m_j is the mass of the jth floor; h_i is the height of the ith floor measured from the base; φ_{j1} is the amplitude at the jth floor of the first mode; and n is the number of stories. The aspect ratio of the building is defined as $\bar{H}/r$, where r is the equivalent foundation radius. The structure-to-soil stiffness ratio a_0 and the structure-to-soil stiffness ratio $\bar{H}/r$ are usually considered as the governing parameters that influence the extent of SSI effects [34, 39]. Other interacting parameters used in this study are as follows:

- Inter-story displacement ductility demand: $\mu = \delta_m / \delta_y$, where δ_m is the maximum inter-story displacement under a specific earthquake excitation and δ_y is the story yield displacement that can be easily calculated based on an equivalent bilinear story shear vs. inter-story drift curve [40]. For MDOF buildings, μ is referred to as the greatest value among all story ductility ratios.

- Structure-to-soil mass ratio: $\bar{m} = m_{tot} / \rho r^2 H$, where H is the total height of the structure, m_{tot} is the total mass of the structure, and ρ is the soil density.

- Foundation-to-structure mass ratio: m_f / m_{tot}, where m_f is the foundation mass. In the present study, m_f is assumed to be equal to the story mass of the MDOF building.

- Poisson's ratio of the soil: υ, which depends on the soil characteristics.

- Damping ratio of the superstructure ζ_s and soil material ζ_0.

In the present study, the Poisson's ratio is considered to be 0.45 for all selected soil-structure systems. However, the effect of using different values of υ on optimum load patterns is also investigated. A damping ratio of 5% is assigned to the soil material.

5. CODE-SPECIFIED SEISMIC DESIGN LOADING PATTERN FOR FIXED-BASE BUILDINGS

The general formula of the lateral design load pattern specified by current seismic codes such as IBC-2012 [2] and ASCE/SEI 7-10 [7] is defined as:

$$F_i = \frac{w_i h_i^k}{\sum_{j=1}^{n} w_j h_j^k} \cdot V_b \qquad\qquad (6)$$

where F_i and V_b are, respectively, the lateral load at the ith level and the total design lateral force (base shear); w_i is the weight of the ith story; and k is a code specific exponent to take into account higher mode effects. According to IBC-2012 [2] (and ASCE/SEI 7-10 [3]), k depends on the fundamental period of the structure (k=1 for periods equal to or less than 0.5 seconds, and k=2 for periods above 2.5 seconds). Note that when k is equal to 1, the obtained lateral load pattern corresponds to an inverted triangular distribution, since the response of the building is assumed to be controlled primarily by the first mode. While k equal to 2 corresponds to a parabolic lateral load pattern with its vertex at the base as the response is assumed to be influenced by higher mode effects.

6. OPTIMUM LATERAL FORCE DISTRIBUTION FOR SOIL-STRUCTURE SYSTEMS

In this section, the optimization algorithm adopted by Ganjavi and Hao [29] for elastic structures is further developed to take into account the inelastic behaviour of soil-structure systems. In this approach, the structural properties are modified so that inefficient material is gradually shifted from strong to weak parts of the structure until a state of uniform damage is achieved. In the present study, inter-story displacement ductility ratio (μ) is used to quantify the structural damage at each story (i.e. damage index). The following step-by-step optimization algorithm is proposed to obtain optimum lateral force distributions for seismic design of non-linear soil-structure systems:

1. Define the MDOF shear-building model based on the height of the prototype structure and number of stories.

2. Select design parameters T_{fix}, ζ_S, ζ_0, $\bar{H}/r$ and a_0 based on the characteristics of the prototype structure and soil condition.

3. An arbitrary pattern for primary height-wise distribution of strength and stiffness are considered along the height of the structure (e.g. uniform distribution). To achieve the target ductility demand, the strength and stiffness of the storeys will be revised in the following steps.

4. Select the target inter-story ductility ratio (μ_t) for the MDOF soil-structure system.

5. Select a spectrum compatible earthquake ground motion that is representative of the design response spectrum over the period range from 0.2 T_i to 1.5 T_i, where T_i is the fundamental period of the fixed-base structure.

6. Calculate the fundamental period of the fixed-base structure (T_i) and scale the total stiffness without altering the stiffness distribution pattern such that the structure has the specified target fundamental period (T_t). The following equation is used for scaling the lateral stiffness of the structure to reach the target period:

$$(\sum_i^n K_j)_{i+1} = (\frac{T_i}{T_t})^2 . (\sum_{i=1}^n K_j)_i \tag{7}$$

where K_j, T_i and T_t are lateral stiffness of the jth story, fixed-base period in the ith step and the target fixed-base period, respectively. At each step, the effective height of the structure, $\bar{H}$, is refined based on the fundamental modal properties of the fixed-base MDOF structure (Eq. 5).

7. Calculate soil parameters for the cone model (Eqs. 1-4)

8. Perform non-linear dynamic analysis on the soil-structure system under the selected design ground motion and calculate the maximum ductility demand μ_{max}. If μ_{max} is close enough to the pre-defined target ductility ratio μ_t (e.g. within 0.5% accuracy), no iteration is necessary. Otherwise, the total base shear strength V_{bs} is scaled, by using the following equation, until the target ductility ratio is achieved.

$$(V_{bs})_{i+1} = (V_{bs})_i (\frac{\mu_{max}}{\mu_t})^\beta \tag{8}$$

where $(V_{bs})_i$ is the total base shear strength of the MDOF system at i^{th} iteration; μ_t and μ_{max} are respectively the target ductility ratio and maximum story ductility ratio among all stories. β is a convergence factor ranging from 0 to 1. The results of this study indicate that, to achieve the best convergence, appropriate values of β are mainly a function of the fundamental period of the fixed-base structure, T_{fix}, rather than the level of inelasticity and the earthquake excitation. It is found that for elastic systems, a very fast convergence (usually less than 5 iterations) can be achieved by using β equal to 0.8. For inelastic systems (i.e. $\mu_t > 1$), however, the best β value can be approximately defined as:

$$\begin{aligned} \beta &= 0.05 - 0.1 & T_{fix} &\leq 0.5 \\ \beta &= 0.1 - 0.25 & 0.5 &< T_{fix} < 1.5 \\ \beta &= 0.25 - 0.4 & T_{fix} &> 1.5 \end{aligned} \tag{9}$$

9. Calculate the Coefficient of Variation (COV) of story ductility ratios along the height of the structure and compare it with the target value of interest, which is considered here 0.02. If the calculated COV is less than the target value, the current pattern is regarded as optimum. Otherwise, the story shear strength and stiffness patterns are modified until the COV decreases to the target value.

10. Stories in which the ductility demand is less than the predefined target value are identified and their shear strength and stiffness are reduced. To obtain a fast convergence in numerical computations, the equation proposed by Hajirasouliha and Moghaddam [14] for fixed-base structures is revised for soil-structure systems as follows:

$$[S_i]_{q+1} = [S_i]_q \cdot [\frac{\mu_i}{\mu_t}]^\alpha \tag{10}$$

where $[S_i]_q$ is the shear strength of the ith floor at q^{th} iteration, μ_i is the story ductility ratio of the ith floor and α is a convergence parameter ranging from 0 to 1. This factor is dependent on the design earthquake excitation and dynamic properties of the structure (e.g. fundamental period and level of inelasticity) and to a less extent on the soil flexibility. Based on intensive analyses performed in the present study, it is concluded that for non-linear soil-structure systems an acceptable convergence is usually obtained by using α= 0.07 for $\mu_t \leq 3$ and α= 0.1 for $\mu_t > 3$.

11. Calculate the maximum story ductility ratio (μ_{max}) of the new soil-structure system under the design earthquake and refine the total base shear strength until μ_{max} is close enough to the target ductility μ_t (e.g. within 0.5% accuracy) by using Eq. 8.

12. Calculate the current fixed-base period T_{fix} and scale the lateral stiffness of the system to reach the target fixed-base period by using Eq. 7.

13. Calculate the current effective height ($\bar{H}$) based on the fundamental mode properties of the new soil-structure system by using Eq. 5.

14. Calculate the current Rayleigh-type damping coefficients to achieve the predefined damping ratios.

15. Convert the optimum shear strength pattern to its corresponding lateral force pattern.

This process is repeated from Step 8 until the COV of story ductility demands in Step 9 is small enough, which implies the optimum design solution is practically achieved. Using the proposed optimization method, the optimum load patterns are obtained for a wide range of target ductility demands, fixed-base periods, non-dimensional frequencies (a_0), aspect ratios ($\bar{H}/r$), number of stories and earthquake excitations. The flowchart of the proposed optimisation method is illustrated in Figure 3. It should be noted that the results presented in this paper are based on IBC-2012 design spectrum compatible earthquakes. However, the proposed methodology can be efficiently used for any set of earthquakes representing a code design spectrum.

7. OPTIMUM SEISMIC DESIGN OF BUILDINGS BY CONSIDERING SSI EFFECTS

To show the efficiency of the proposed method for optimum seismic design of non-linear soil-structure systems, the above algorithm is applied to a 10-story shear building with $T_{fix} = 1.5$ sec, $\mu_t = 6$, $\bar{H}/r = 3$, and $a_0 = 2$ subjected to Kobe (Shin Osaka) earthquake. Figure 4a illustrates a comparison of IBC-2012 [2] (or ASCE/SEI 7-10 [3]) design load pattern with the optimum pattern for fixed-base and soil-structure systems. It is shown that the optimum design load patterns, in general, can be very different from code-specified patterns. On the other hand, a significant difference is observed between the optimum pattern of the soil-structure system and that of the fixed-base structure, which highlights the effects of SSI on the optimum design load pattern. The height-wise distribution of story ductility demands resulted from utilizing these lateral load patterns are depicted in Figure 4b. It can be seen that while using the SSI optimum pattern results in a completely uniform distribution of the deformation, using the code-specified and fixed-base optimum patterns leads to a non-uniform distribution of ductility demands along the height of the soil-structure system. The Coefficient of Variation (COV) of story ductility demands resulted from applying IBC-2012 [2], fixed-base optimum and SSI optimum patterns are calculated 94%, 64% and 0.3%, respectively. This implies that utilizing code-specified and fixed-base optimum load patterns may not result in an optimum seismic performance of soil-structure systems in inelastic range of vibration. To examine the effect of non-linear behaviour of SSI systems, the above process was repeated for the same earthquake and shear building model but in elastic range of response (i.e. $\mu_t=1$). The COV of story ductility demands obtained in this case were 22.6%, 19.6% and 0.3% for IBC-2012 [2], fixed-base optimum and SSI optimum patterns, respectively. This indicates that the effect of SSI on the optimum design load pattern is more significant in inelastic range of response when compared to the elastic state.

The efficiency of the proposed optimum load patterns can also be investigated by comparing the required structural weight (or weight index) to satisfy a prescribed target ductility demand under the selected design earthquake ground motion. In this study, the structural weight index for a specific structure is defined as the total weight of the seismic resistant system (proportional to the total story shear strength) normalized by the total weight of the structure and PGA [29]. The loading pattern that leads to a minimum weight index is considered as the most adequate (or optimum) design pattern [14, 15, 29]. Figure 5 shows the reduction of the structural weight in optimum structures with respect to those designed based on IBC-2012 [2] for 10-story soil-structure systems with $\bar{H}/r = 3$ and low ($\mu = 2$) and high ($\mu = 6$) ductility levels. It is clearly seen that even for the case of low SSI effect (i.e. $a_0 =1$), optimum structures experience up to 55% less structural weight as compared with their code-based counterparts. As expected, the efficiency of the optimum patterns is more pronounced for the structures with longer periods, in which higher mode effect is predominant.

As discussed before, the COV of story ductility demands can be used to assess the efficiency of different design load patterns, since more uniform distribution of ductility demands usually leads to a better seismic performance [10, 12, 14]. To this end, the COV of story ductility demands of fixed-base and soil-structure systems designed according to IBC-2012 [2] and optimum load patterns are compared in Figure 6 for different fundamental periods, soil flexibility and ductility levels (average of the 21 earthquakes). It is shown that the mean COV of story ductility demands of optimum design soil-structure systems is always less than 3%, which means a uniform damage distribution is practically achieved. It is observed that for the structures designed with IBC-2012 load pattern, increasing the soil flexibility and target ductility is generally accompanied by an increase in the mean percentage of COV of story ductility demands. This implies that the efficiency of the code-specified lateral load patterns, in general, decreases by increasing SSI effects and nonlinearity of the structures.

8. EFFECTS OF KEY DESIGN PARAMETERS ON OPTIMUM LATERAL LOAD PATTERNS

The effects of various design parameters including the dynamic characteristics of the superstructure, SSI interacting parameters and design earthquake excitation on optimum lateral load distributions of non-linear SSI systems are investigated in this section.

8.1. Effect of Fundamental Period

To study the effect of fundamental period on the optimum load pattern of inelastic soil-structure systems, 10-story shear building models with $\bar{H}/r = 3$ and $a_0 = 2$ having fixed-base fundamental periods of 0.5, 1, 2 and 3 sec are considered. For each soil-structure system, optimum load patterns are derived for $\mu_t = 2$ and 6 representing low and high ductility levels, respectively. Figure 7 shows the average of the results under the 21 selected earthquake ground motions (see Table 1). As seen, the average optimum load pattern is significantly dependent on the fundamental period of the superstructure for both low and high ductility levels. For low ductility levels (i.e., $\mu_t = 2$), increasing the fundamental period is mostly accompanied by increasing the lateral shear force at top stories, which can be interpreted as the effect of higher modes. The only exception is for the case of very long period structures ($T_{fix} = 3$ sec), where the lateral force increases at both top and bottom stories. However, when the plastic deformation is significant (i.e., $\mu = 6$), increasing the fundamental period is generally accompanied by increasing the lateral shear force at both top and bottom stories (more pronounced in bottom stories). It should be noted that previous studies carried out by Moghaddam and Hajirasouliha [11] and Hajirasouliha and Moghaddam [14] showed that increasing the fundamental period of fixed-base shear-building structures is only accompanied by increasing the shear strength at top stories. Therefore, it can be concluded that SSI affects the optimum lateral load patterns in different ways when compared with fixed-base systems.

8.2. Effect of Target Ductility Demand

Figure 8 shows the effect of target ductility demand on the average optimum load pattern of non-linear soil-structure systems subjected to the 21 selected ground motions. For this purpose, 10-story shear-building models with $\bar{H}/r = 3, a_0 = 2$, fixed-base fundamental periods of 0.5 and 2 sec (representing rigid and flexible structures) and target ductility demands of 1, 2, 4 and 6 have been considered. It is shown that for both rigid and flexible models, the average optimum lateral load pattern is significantly affected by the target ductility demand while nearly in all code-specified seismic load patterns the effect of this parameter is ignored. It can also be seen that for soil-structure systems, increasing the target ductility demand is accompanied by a decrease and an increase in story shear strength at top and bottom stories, respectively. This observation is consistent with the findings of Hajirasouliha and Pilakoutas [15] for fixed-base shear-building structures.

8.3. Effect of Number of Stories

To examine the effect of number of stories on the optimum load distribution pattern, the proposed optimization algorithm is applied to the 5-, 10-, 15- and 20-story soil-structure models with $T_{fix} = 1.5$ sec, $\bar{H}/r = 3$ and $a_0 = 2$. Figure 9 presents the average of the results for the 21 selected earthquake ground motions. In order to compare the optimum load patterns corresponding to different number of stories, normalized lateral loads are plotted. The vertical and horizontal axes of Figure 9 are relative height and normalized lateral load divided by base shear, respectively. It can be concluded from this figure that the optimum load patterns are almost independent of the number of stories. This finding is consistent with the results presented by Hajirasouliha and Pilakoutas [15] for fixed-base shear-building structures and Ganjavi and Hao [29] for elastic soil-structure systems.

8.4. Effect of non-dimensional frequency

Figure 10 shows the effect of non-dimensional frequency (structure-to-soil stiffness ratio) a_0 on the average optimum load pattern of soil-structure systems subjected to the 21 selected ground motions. The results are plotted for 10-story shear buildings with fundamental periods of 0.5 and 2 sec, $\bar{H}/r = 3$, and three different non-dimensional frequencies $a_0 = 1, 2, 3$. It can be observed that, in general, a_0 can considerably affect the average optimum load pattern of non-linear soil-structure systems compared to their fixed-based counterparts. For rigid structures (i.e., $T_{fix} = 0.5$ sec), increasing a_0 results in increasing the lateral load at top stories and decreasing the load at lower stories. However, for flexible structures (i.e., $T_{fix} = 2$ sec), increasing a_0 is mainly accompanied by increasing the lateral load at both bottom and top

stories, and decreasing the load at middle stories. This phenomenon can be due to increasing the effect of SSI in the systems with higher non-dimensional frequency a_0.

8.5. Effect of Aspect ratio

The aspect ratio (slenderness ratio) of the superstructure is another key parameter that can affect the optimum lateral design load pattern of the soil-structure system. Figure 11 compares the average optimum load pattern of 10-story systems with T_{fix} =1.5 sec, ductility demand of 4, non-dimensional frequencies a_0 =1, 3 (representing insignificant and severe SSI effects) and aspect ratios $\bar{H}/r$ = 1, 3, 5 (representing squat, average and slender buildings). It is shown in Figure 11(a) that for the systems with insignificant SSI effect (i.e. a_0 =1), increasing the aspect ratio $\bar{H}/r$ will not considerably change the average optimum design load pattern. However, Figure 11(b) shows that by increasing the non-dimensional frequency a_0, the aspect ratio can play a more important role. In soil-structure systems with severe SSI effect (i.e. a_0 =3), increasing the aspect ratio is accompanied by increasing the lateral load at the top and lower stories, and decreasing the load in the middle stories. This phenomenon is more pronounced for slender building (i.e. $\bar{H}/r$ = 5). This implies that the effect of SSI on average optimum lateral load pattern will become more significant for slender buildings with large non-dimensional frequency (i.e. on soft soil profiles). A similar conclusion has been reported by Ganjavi and Hao [29] for elastic soil-structure systems.

8.6. Effect of Structural Damping Ratio and Damping Model

The effect of structural damping ratio on the optimum design load pattern of soil-structure systems is illustrated in Figure 12(a) for a 10-story shear-building structure with T_{fix} = 1.5, μ_t = 6, $\bar{H}/r$ = 3 and a_0 = 2 subjected to Loma Prieta earthquake (APEEL 2- Redwood City) using four different damping ratios ζ_S =0.5%, 3%, 5% and 10%. The results indicate that, for practical purposes, the optimum design load patterns of non-linear soil-structure systems can be considered insensitive to the variation of structural damping ratio.

To investigate the effect of structural damping model, the optimum design load pattern of the above 10-story shear-building structure was calculated using three different viscous damping models including stiffness-proportional damping, mass-proportional damping and Rayleigh-type damping model (superposition of mass and stiffness proportional damping terms). The optimum lateral load patterns corresponding to each damping model (ζ_S = 5%) are compared in Figure 12(b). It is expected that Rayleigh-type damping model leads to more reliable results as it can better incorporate the effect of higher modes [8]. It is shown in Figure 12 (b) that there is no significant difference between the results of mass-proportional and Rayleigh-type damping models, however, the difference is pronounced when compared

to the stiffness-proportional damping model. Similar results have been obtained for soil-structure models subjected to other seismic ground motions. This observation indicates that the stiffness-proportional damping model may not lead to accurate predictions of structural responses in soil-structure systems as compared to the Rayleigh damping model.

While the convergence of the optimization problem is found not to be very sensitive to the variation of damping ratio, it is to a large extent sensitive to the type of selected damping model. The results of this study indicate that generally more iteration steps are required for optimization of structures designed based on mass-proportional and Rayleigh-type damping models compared to the stiffness-proportional damping model. It is also found that to achieve a stable convergence, the convergence parameter α needs to be decreased, respectively, when structures are designed based on stiffness-proportional, Rayleigh-type and mass-proportional damping models. As an instance, for the case of $\mu_t = 3$, the suitable values of α are approximately 0.2, 0.07 and 0.05 when stiffness-proportional, Rayleigh-type and mass-proportional damping models are employed, respectively.

8.7. Effect of Structural Strain Hardening

The effect of using different structural strain hardening (SH) values on the optimum design load pattern of soil-structure systems is investigated in Figure 13. The results are plotted for the same soil-structure model and earthquake ground motion record as Figure 12 but for two different ductility demands of 2 and 6 representing low and high levels of nonlinearity. For this case, four different strain hardening values of 0%, 2%, 5% and 10% are considered. It can be seen that while optimum load patterns are practically independent of the selected structural strain hardening in low inelasticity levels (i.e. μ= 2), they can be more sensitive to the variation of the structural strain hardening in soil-structure systems with high level of nonlinearity (i.e. μ= 6).

8.8. Effect of Soil Poisson's Ratio

Figure 14 shows the effect of soil Poisson's ratio on the optimum load pattern of soil-structure systems. The results are for 10-story shear buildings with T_{fix} =1.5 sec, two ductility levels of 2 and 6, non-dimensional frequency of 3 (severe SSI effect) and aspect ratio of 3 subjected to Loma Prieta earthquake (APEEL 2- Redwood City). It can be observed that optimum lateral load patterns, in general, are sensitive to the variation of Poisson's ratio only in low ductility levels. However, the optimum lateral load pattern can be considered to be independent of the soil Poisson's ratio when structures undergo significant plastic deformations (e.g. under strong earthquakes).

8.9. Effect of Earthquake Excitation

To examine the effect of design earthquake on the optimum lateral force pattern of soil-structure systems in inelastic range of response, the individual results of the 21 selected earthquake ground motions along with their mean values are presented in Figure 15. The results are for 20- story shear building systems with T_{fix} = 2 sec, μ= 4, aspect ratio of 3, and non-dimensional frequency of 2. It is clear from the results that the optimum strength distribution pattern in some cases is sensitive to the earthquake ground motion characteristics. However, it is expected that utilizing the mean pattern will lead to acceptable designs although some inevitable variation is not avoidable depending on the earthquake ground motions characteristics.

Figure 16 illustrates the effect of ground motion intensity on the optimum load pattern of a 10-story soil-structure model with T_{fix} =1.5 sec, μ =4, $\bar{H}/r$ =3, and $a_0 = 2$ subjected to Kobe (Shin Osaka) earthquake with the PGA multiplied by 0.5, 1, 2, and 3 intensity factors (SF). The results indicate that for a specific fundamental period, aspect ratio and non-dimensional frequency, the optimum lateral load pattern is completely independent of the ground motion intensity factor, which is consistent with the findings of Mohammadi et al. [10] and Hajirasouliha and Moghaddam [14] for fixed-base shear-building structures. It should be noted that this conclusion was expected as the target ductility demand was kept unchanged for all ground motion intensity levels.

The general loading patterns presented in this article should be efficient for structural systems that exhibit shear-building like behaviour, such as concentrically braced frames and moment resisting frames with high beam-to-column stiffness ratio. However, the results cannot be directly applied to some structural systems such as structural walls, as they behave substantially different from shear-building type of structures.

9. CONCLUSIONS

In this study, a practical optimization technique is developed to obtain optimum lateral load distribution for seismic design of non-linear shear buildings by considering soil-structure interaction (SSI) effects. It is shown that the optimum design lateral load pattern of flexible-base structures with SSI is highly dependent on the fundamental period, target ductility demand, non-dimensional frequency, aspect ratio, seismic excitation and structural damping model. However, the results indicate that the optimum design load pattern is less affected by structural post-yield behaviour and soil Poisson's ratio and is almost independent of the number of stories, structural damping ratio and earthquake intensity. While the convergence of the optimization problem is not very sensitive to the variation of damping ratio, the results

indicate that, in general, more iteration steps are required for optimization of structures designed based on the mass-proportional and the Rayleigh-type damping models compared to the stiffness-proportional damping model. The efficiency of the proposed optimization algorithm is investigated by comparing the structural weight index and COV of story ductility demands of a wide range of optimum and code-based design models. It is shown that, to satisfy a predefined target ductility demand, SSI systems designed with the optimum design load patterns require up to 55% less structural weight compared to those designed based on IBC-2012 [2] (or ASCE/SEI 7-10 [3]) load patterns. The efficiency of the optimum load patterns is more pronounced for the structures with longer periods, in which higher mode effect is dominant. Although the results of this study are limited to the shear buildings with shallow foundations, the general outcomes should prove useful for preliminary design of multi-story structures on soft soil profiles.

ACKNOWLEDGMENTS

REFERENCES

[1] CEN 2003. EuroCode 8: Design of structure for earthquake resistance – Part 1: General rules for buildings. Bruxelles: European Committee for Standardization; 2003.

[2] IBC-2012, International Code Council (ICC), International Building Code, Birmingham, AL; 2012.

[3] ASCE/SEI 7-10, Minimum Design Loads for Buildings and Other Structures. American Society of Civil Engineers: Reston, VA; 2010.

[4] Building Seismic Safety Council (BSSC). National Earthquake Hazard Reduction Program (NEHRP) Recommended Provisions for Seismic Regulations for 348 New Buildings and Other Structures-Part 2: Commentary (FEMA 450-2). Federal Emergency Management Agency, Washington, D. C.; 2003.

[5] Uniform Building Code (UBC), Int. Conf. of Building Officials, Vol. 2, California; 1994.

[6] Anderson JC, Miranda E, Bertero VV. Evaluation of the seismic performance of a thirty-story RC building, UCB/EERC-91/16, Earthquake Engineering Research Centre, University of California, Berkeley; 1991.

[7] Gilmore TA, Bertero VV. Seismic performance of a 30-story building located on soft soil and designed according to UBC 1991. UCB/EERC-93/04. Earthquake Engineering Research Center, University of California, Berkeley; 1993.

[8] Chopra AK. Dynamics of Structures- Theory and Applications to Earthquake Engineering. 4th edition, Prentice Hall, Englewood Cliffs, New Jersey, 2012.

[9] Leelataviwat S, Goel SC, Stojadinovic B., 1999. Toward performance-based seismic design of structures. Earthquake Spectra 1999; 15(3): 435–461.

[10] Mohammadi KR, El-Naggar MH, Moghaddam H. Optimum strength distribution for seismic resistant shear buildings. Int. J. Solids Struct. 2004; 41(21-23): 6597–6612.

[11] Moghaddam H, Hajirasouliha I. Toward more rational criteria for determination of design earthquake forces. International Journal of Solids and Structures 2006; 43(9): 2631–2645.

[12] Moghaddam H, Hajirasouliha I. Optimum strength distribution for seismic design of tall buildings. Struct. Design Tall Spec. Build. 2008; 17: 331–349.

[13] Ganjavi B, Vaseghi AJ, Ghodrati AG, Yahyazadeh AQ. Distribution of Drift, Hysteretic Energy and Damage in Reinforced Concrete Buildings with Uniform Strength Ratio. In: The 14th World Conf. on Earthquake Engineering, Beijing, China; 2008.

[14] Hajirasouliha I, Moghaddam H. New lateral force distribution for seismic design of structures. J. Struct. Eng. ASCE 2009; 135(8): 906–915.

[15] Hajirasouliha I, Pilakoutas K. General seismic load distribution for optimum performance-based design of shear-buildings. Journal of Earthquake Engineering 2012; 16(4): 443-462.

[16] Lee SS, Goel SC, 2001. Performance-Based Design of Steel Moment Frames Using Target Drift and Yield Mechanism, Report No. UMCEE 01-17, Department of Civil and Environmental Engineering, University of Michigan; 2001.

[17] Goel SC, Liao WC, Bayat MR, Chao SH. Performance-Based Plastic Design (PBPD) Method for Earthquake-Resistant Structures: An Overview. Structural Des. Tall Spec. Build. 2010; 19 (1-2): 115-137.

[18] Hajirasouliha I, Asadi P, Pilakoutas K. An efficient performance-based seismic design method for reinforced concrete frames. Earthquake Engng. Struct. Dyn. 2012; 41: 663–679.

[19] Ghannad MA, Jahankhah H. Site dependent strength reduction factors for soil–structure systems. Soil Dyn. Earthquake Eng. 2007; 27(2): 99–110.

[20] Ganjavi B, Hao H. Strength reduction factor for MDOF soil-structure systems. The Structural Design of Tall and Special Buildings 2014; 23(3): 161-180.

[21] Barcena A, Esteva L. Influence of dynamic soil–structure interaction on the nonlinear response and seismic reliability of multistory systems. Earthquake Eng. Struct. Dyn. 2007; 36(3): 327-346.

[22] Tang Y, Zhang J. Probabilistic seismic demand analysis of a slender RC shear wall considering soil–structure interaction effects. Engineering Structure 2001; 33(1): 218–229.

[23] Raychowdhury P. Seismic response of low-rise steel moment-resisting frame (SMRF) buildings incorporating nonlinear soil–structure interaction (SSI). Eng Struct. 2011; 33(3): 958–967.

[24] Aviles J, Perez-Rocha JL.Use of global ductility for design of structure–foundation systems. Soil Dyn. Earthquake Eng. 2011; 31(7): 1018–1026.

[25] Khoushnoudian F, Ahmadi E. Effects of pulse period of near-field ground motions on the seismic demands of soil-MDOF structure systems using mathematical pulse models. Earthquake Eng. Struct. Dyn 2013; 42(11): 1565-1582.

[26] Abedi NF, Khoshnoudian F. Evaluation of ground motion scaling methods in soil–structure interaction analysis. Struct. Design Tall Spec. Build 2014; 23: 54–66.

[27] Ghannad MA, Jafarieh AH. Inelastic displacement ratios for soil–structure systems allowed to uplift. Earthquake Engng. Struct. Dyn. 2014; 43: 1401–1421.

[28] Ganjavi B, Hao H. A parametric study on the evaluation of ductility demand distribution in multi-degree-of freedom systems considering soil–structure interaction effects. Engineering Structures 2012; 43:88–104.

[29] Ganjavi B, Hao H. Optimum lateral load pattern for seismic design of elastic shear-buildings incorporating soil–structure interaction effects. Earthquake Engng. Struct. Dyn. 2013; 42: 913–933.

[30] Bolourchi, S. A, Optimum seismic design of shear-buildings with soil–structure interaction effects. MSc thesis. Sharif University of Technology 2007.

[31] FEMA 440. Improvement of nonlinear static seismic analysis procedures. Report No. FEMA 440, Federal Emergency Management Agency, prepared by Applied Technology Council; 2005.

[32] SeismoMatch. A computer program for adjusting earthquake records to match a specific target response spectrum; 2014 (Available from: http://www.seismosoft.com)

[33] Hancock J, Watson-Lamprey J, Abrahamson NA, Bommer JJ, Markatis A, McCoy E, Mendis R. An improved method of matching response spectra of recorded earthquake ground motion using wavelets. Journal of Earthquake Engineering 2006; 10(1): 67–89.

[34] Wolf JP. Foundation Vibration Analysis using Simple Physical Models. Prentice-Hall: Englewood Cliffs, NJ; 1994.

[35] Wolf JP, Deeks AJ. Foundation Vibration Analysis: A Strength-of-Materials Approach. Elsevier: Burlington, MA; 2004.

[36] Kramer Sl. Geotechnical earthquake engineering. Englewood Cliffs (NJ): Prentice-Hall; 1996.

[37] Veletsos AS. Dynamics of structure–foundation systems. In: Structural and Geotechnical Mechanics, Hall WJ (ed.), A Volume Honoring N.M. Newmark. Prentice-Hall: Englewood Cliffs, NJ, 333–361; 1977.

[38] Stewart JP, Seed RB, Fenves GL. Seismic soil-structure interaction in buildings II: Empirical findings. Journal of Geotechnical and Geoenvironmental Engineering (ASCE) 1999; 125(1): 38-48.

[39] Veletsos AS, Meek JW. Dynamic behavior of building–foundation system. Earthquake Eng. Struct. Dyn.1974; 3(2): 121–138.

[40] Hajirasouliha I, Doostan A. A simplified model for seismic response prediction of concentrically braced frames. Advances in Engineering Software 2010; 41(3): 497-505.
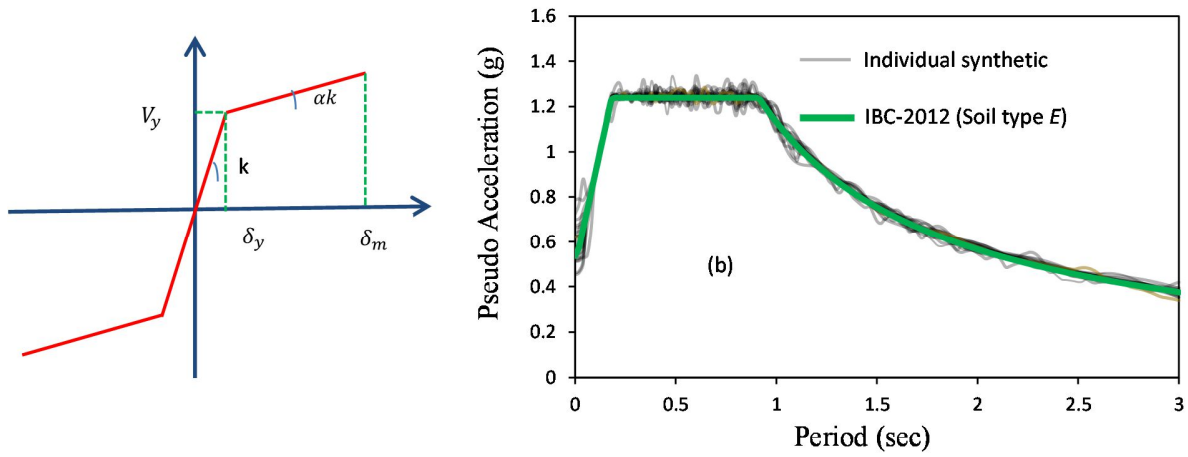
Figure 1. (a): Bilinear Elasto-plastic model for force-displacement relationship; (b): IBC-2012 (ASCE/SEI 7-10) design spectrum for soil type E and response spectra of 21 adjusted earthquakes (5% damping)
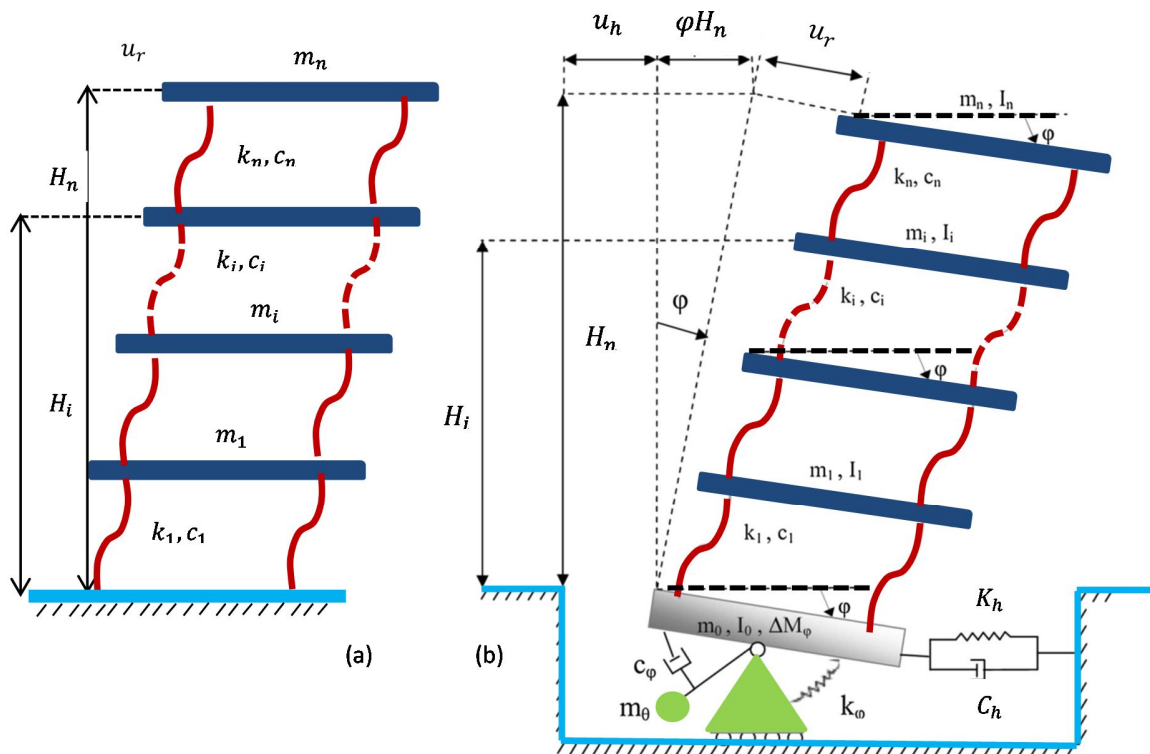
Figure 2. Typical multi-story shear building models (a) fixed-base model and (b) flexible-base model

Select: N, h_i, T_{fix}, ζ_{st}, ζ_0, a_0 and $\bar{H}/r$

$\bar{m} = m_{tot}/\rho r^2 H$

Assign initial stiffness k_{tot} and strength V_{bs}, and distribute them uniformly along the height of the structures

Scale K_{tot} to to reach the target period:
$$(\sum_{i}^{n} K_{j+1})_{i+1} = (\frac{T_i}{T_t})^2 \cdot (\sum_{i=1}^{n} K_j)_i$$

Calculate soil parameters: Eqs. [1-4]

Select target ductility μ_t

Adjust V_{bs} by:
$$(V_{bs})_{i+1} = (V_{bs})_i (\frac{\mu_{max}}{\mu_t})^\beta$$
$\beta = 0.05 - 0.1$ if $T_{fix} \le 0.5$
$\beta = 0.1 - 0.25$ if $0.5 < T_{fix} < 1$
$\beta = 0.25 - 0.4$ if $T_{fix} > 1.5$

Perform nonlinear time history analysis under given earthquake

No

Control the target period:
Is $|T_i - T_t| \le 0.01$?

Yes

Calculate stories ductility μ_i

1. Refine Rayleigh damping coefficients
2. Refine $\bar{H}$ [Eq. 5]

No

Is $|\mu_t - \mu_{max}| \le 0.05\mu_t$?

Yes

Modify story shear strength S_i:
$$[S_i]_{q+1} = [S_i]_q \cdot [\frac{\mu_i}{\mu_t}]^\alpha$$
$\alpha = 0.07$ if $\mu_t \le 3$
$\alpha = 0.1$ if $\mu_t > 3$

Calculate COV for μ_i:
Is COV ≤ 0.02 ?

No

Yes

Convert the optimum shear strength pattern to its corresponding lateral force pattern

Optimum Seismic Design Lateral Load Force

Figure 3. Flowchart showing the general procedure for optimum seismic design of nonlinear building with SSI
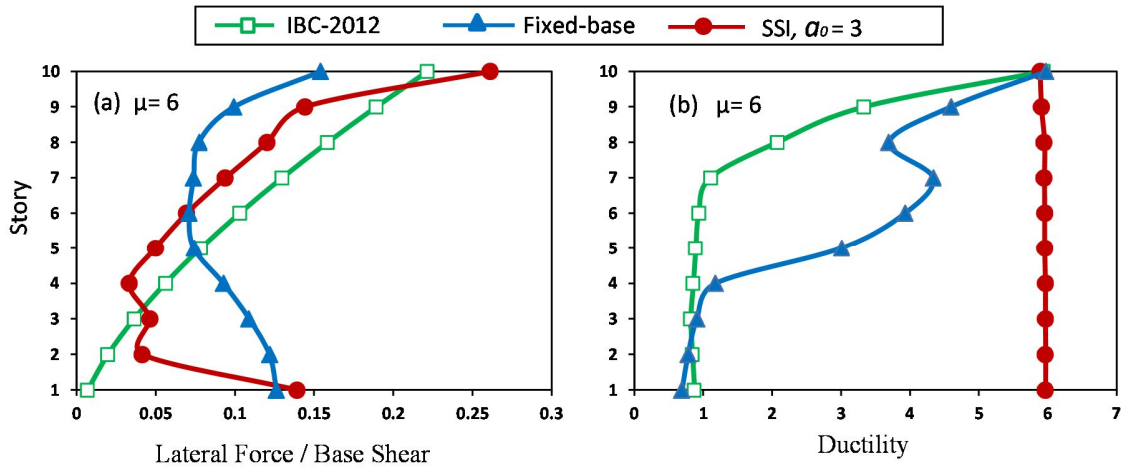
Figure 4. Comparison of IBC-2012 and fixed-base optimum load patterns with optimum designed models of soil-structure system: (a) lateral force distribution; (b) story ductility pattern, 10-story shear building with T_{fix} = 1.5 sec, μ= 6, $\bar{H}/r$ =3, Kobe (Shin Osaka) earthquake
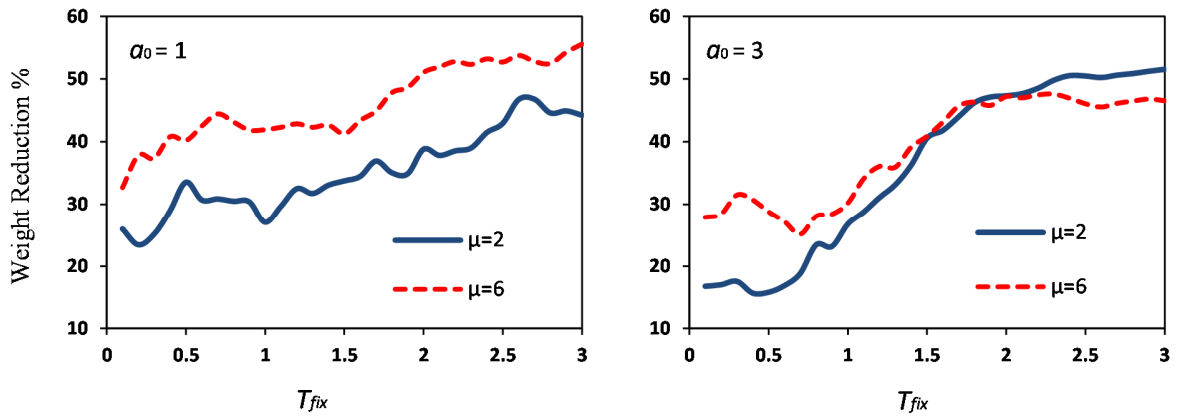
Figure 5. Structural weight reduction of optimum structures with respect to those designed based on IBC-2012 for the 10-story soil-structure systems; average of 21 earthquakes; $\bar{H}/r$ =3
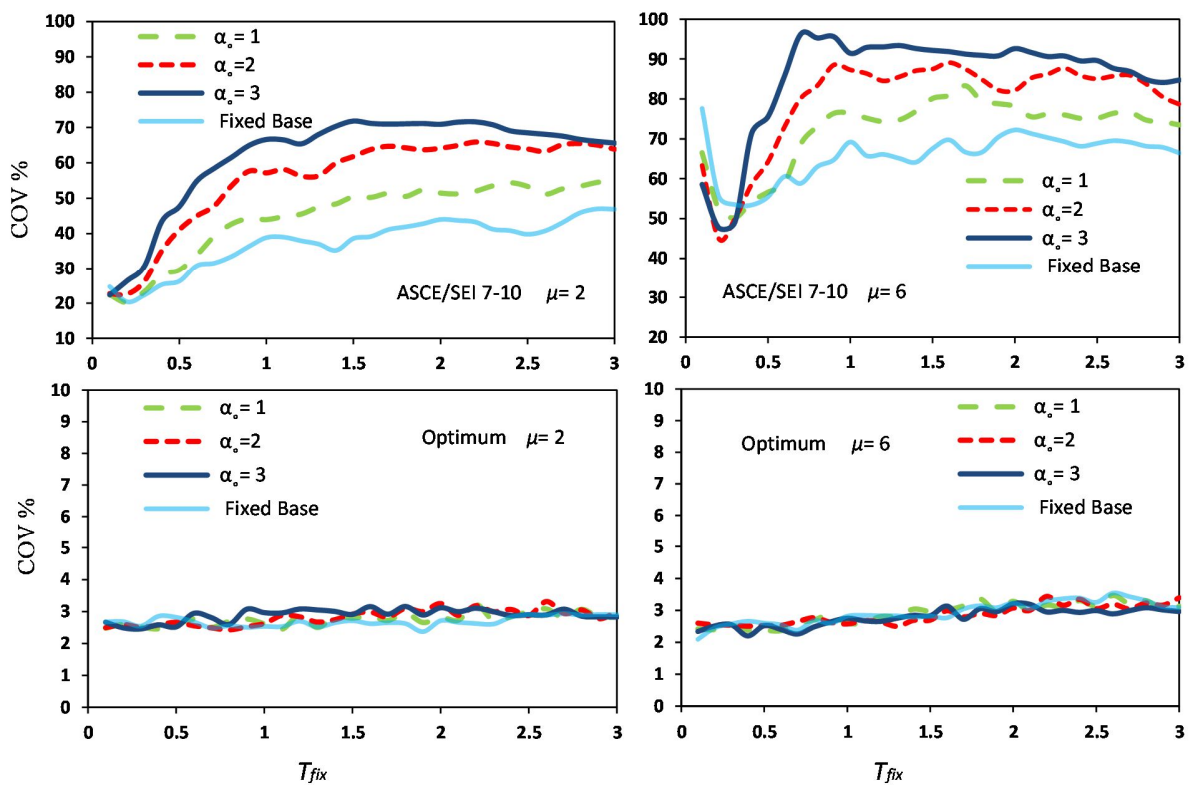
Figure 6. Mean COV% of inelastic fixed- base and soil–structure systems with 20 stories designed according to IBC-2012 and optimum load patterns; average of 21 earthquakes; $\bar{H}/r = 5$
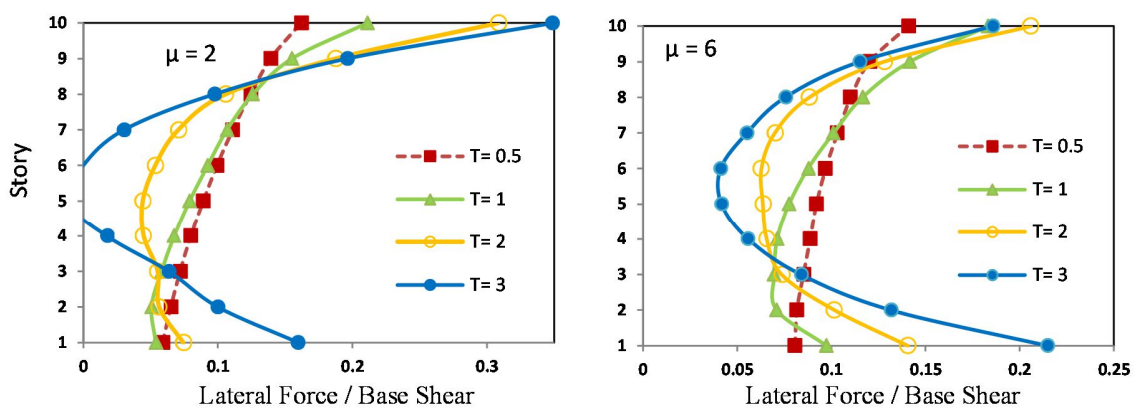
Figure 7. Effect of fundamental period on optimum lateral force distribution for soil-structure systems with $\bar{H}/r = 3$ and $a_0 = 2$; 10-story building (average of 21 earthquakes)
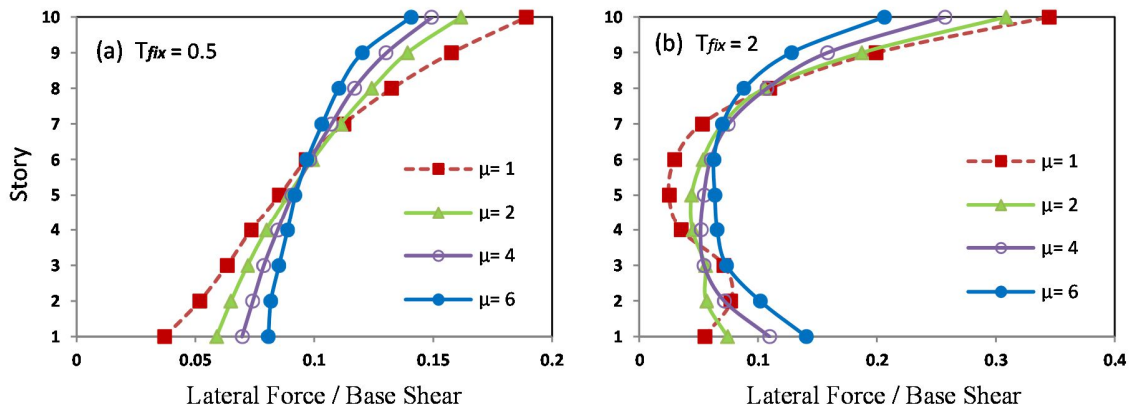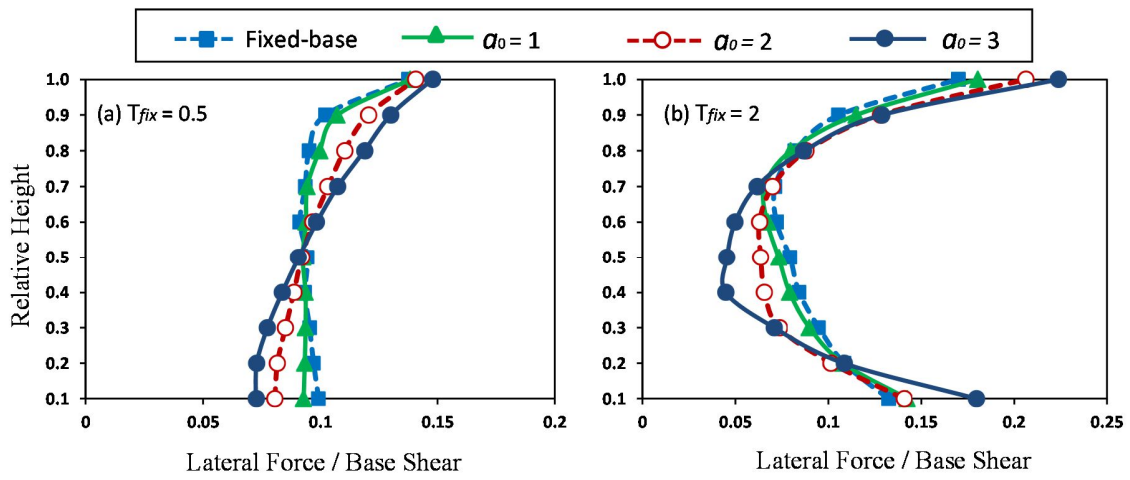
Figure 8. Effect of target ductility demand on optimum lateral force distribution for soil-structure systems with $\bar{H}/r$ = 3 and a_0 = 2; 10-story building (average of 21 earthquakes)
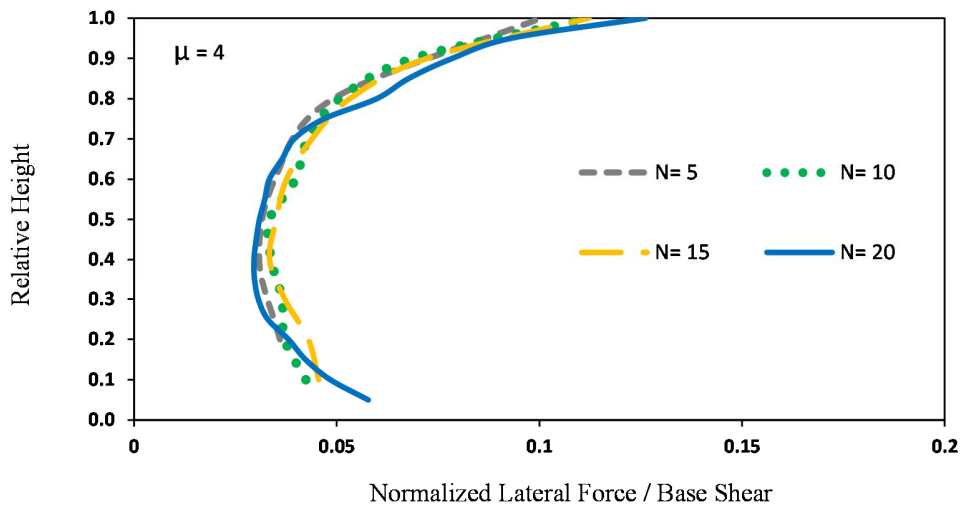
Figure 9. Effect of the number of stories on optimum lateral force distribution for soil-structure systems with $\bar{H}/r$ = 3 and a_0 = 2; T_{fix} = 1.5 sec. (average of 21 earthquakes)

Figure 10. Effect of dimensionless frequency on mean optimum lateral force distribution for 10-story soil-structure systems with $\bar{H}/r$ =3, μ= 6: (a) T_{fix} = 0.5 sec.: (b) T_{fix} = 2 sec.
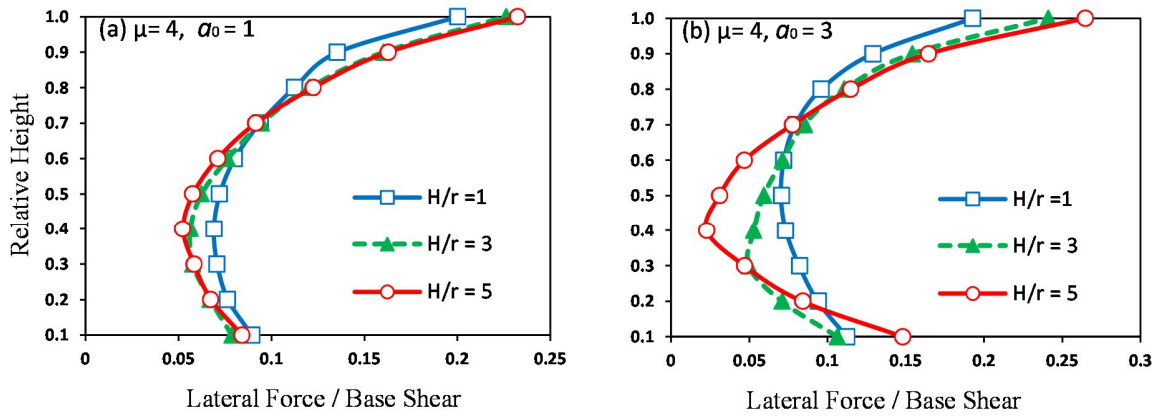
Figure 11. Effect of aspect ratio on optimum lateral force distribution for a 10-story soil-structure system with T_{fix} = 1.5 sec, μ= 4 (average of 21 earthquakes)
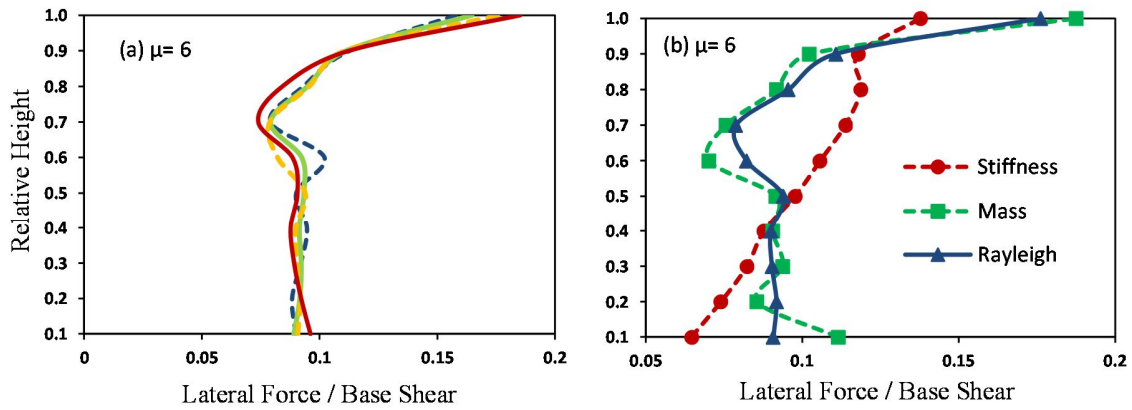
Figure 12. Optimum lateral force distribution for a 10-story soil-structure system with $\bar{H}/r$ =3, $a_0 = 2$, T_{fix} = 1.5 sec and μ= 6: (a) Effect of structural damping ratio; (b) Effect of structural damping model; Loma Prieta (APEEL 2 - Redwood City) earthquake
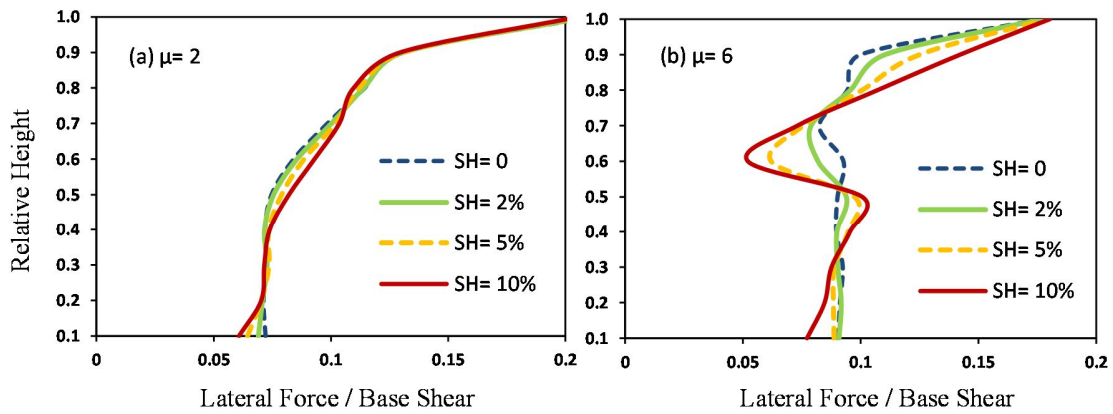

Figure 13. Effect of structural post yield behavior on optimum lateral force distribution for a 10-story soil-structure system with $\bar{H}/r$ =3, $a_0 = 2$, T_{fix} = 1.5 sec; Loma Prieta (APEEL 2 - Redwood City) earthquake
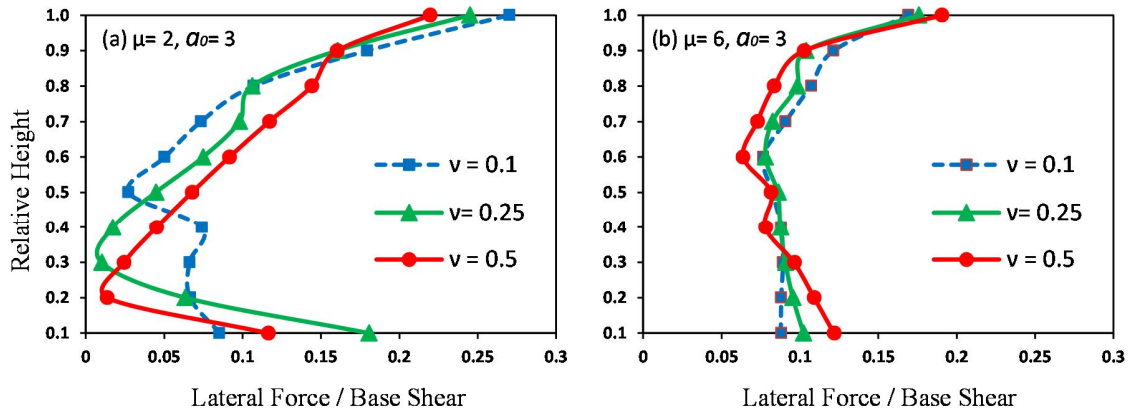
Figure 14. Effect of soil Poisson ratio on optimum lateral force distribution for a 10-story soil-structure system with $\bar{H}/r = 3$, $a_0 = 3$, $T_{fix} = 1.5$ sec; Loma Prieta (APEEL 2 - Redwood City) earthquake
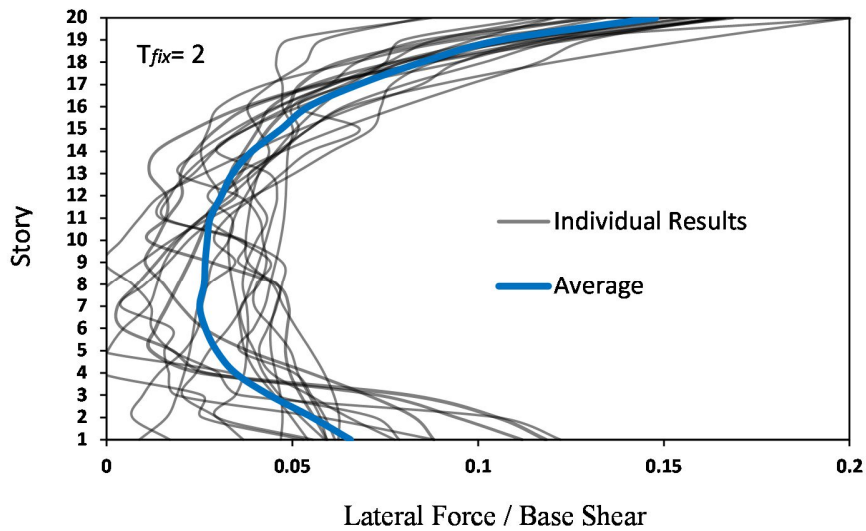

Figure 15. Effect of earthquake excitation on optimum lateral force distribution for a soil-structure system with $\bar{H}/r = 3$, $a_0 = 2$ and $\mu = 4$ under 21 selected earthquakes
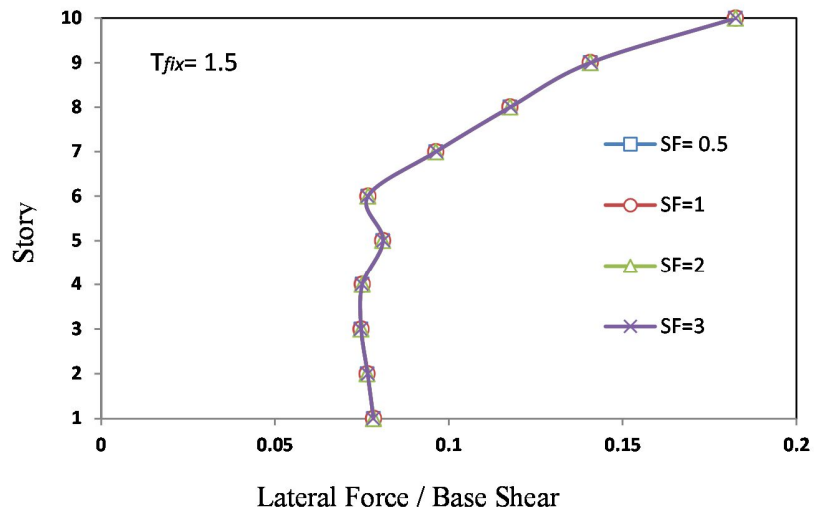
Figure 16. Effect of ground motion intensity on optimum lateral force distribution for soil-structure systems with $\bar{H}/r = 3$ and $a_0 = 2$, $\mu = 4$; Kobe (Shin Osaka) earthquake